AIAA JOURNAL
Vol. 44, No. 3, March 2006

Control of Flow Structure on Delta Wing with Steady Trailing-Edge Blowing

M. M. Yavuz* and D. Rockwell†
Lehigh University, Bethlehem, Pennsylvania 18015

The near-surface flow structure and topology are characterized on a delta wing of low sweep angle, which is subjected to trailing-edge blowing. A technique of high-image-density particle image velocimetry is employed to determine the topological critical points adjacent to the surface and in the near wake of the wing, in relation to the dimensionless magnitude of the blowing coefficient. These topological features are, in turn, interpreted in conjunction with patterns of surface-normal vorticity and near-surface velocity fluctuations, which provide an indication of buffet loading. Even though the jet blowing is at the trailing edge, it has a remarkable, global influence on the surface patterns located well upstream; at high angle of attack, it leads to eradication of large-scale, three-dimensional separation in the vicinity of the apex.

I. Introduction

RECENT interest in unmanned combat air vehicles (UCAVs) has motivated investigation of flow structure on delta wings having low and moderate values of sweep angle. This interest leads us to investigate the control of near-surface flow topology of delta wings having a low sweep angle with steady trailing-edge blowing and the effect of angle of attack of planform and different blowing locations on flow structure. Related investigations that were previously done include experimental and numerical studies of the flow structure above wings of low- and moderate-sweep angle and investigations of blowing concept and its effects on flow structures of delta wings. These are included in the summaries that follow.

A. Flow Structure and Topology on Moderate- and Low-Swept Delta Wings

The generic features of UCAV configurations can be represented by delta wings having low and moderate values of sweep angle. They are associated with distinctive types of flow patterns above and at the surface of the wing, which have been the subject of recent investigations. Ol and Gharib[1,2] undertook experimental investigations of wings of sweep angle $\Lambda = 50$ and 65 deg. They determined the onset of vortex breakdown using dye visualization and, via a stereo particle image velocimetry (PIV) technique, characterized various features of the leading-edge vortex structure. Honkan and Andreopoulos[3] determined patterns of instantaneous vorticity on a delta wing of sweep angle $\Lambda = 45$ deg with triple orthogonal hot-wire probes and identified the existence of discrete stationary vortices in the feeding shear layer as well as the primary vortex. They also showed that high turbulence activity is associated with the regions of shear layer reattachment and secondary separation. Miau et al.[4] investigated the flow patterns on a wing of sweep angle $\Lambda = 50$ deg, with a focus on the consequences of leading-edge profile. The detailed characteristics of the instantaneous and averaged flow structure, as well as the surface flow topology on a delta wing of sweep angle $\Lambda = 50$ deg, were numerically computed by Gordnier and Visbal.[5] Taylor et al.[6] employed a dye technique, along with complementary particle image velocimetry, to visualize the vortex cores on low swept $\Lambda = 50$ deg wings, and Taylor and Gursul[7] investigated the near-surface topology and buffeting phenomena on the same planform. Both of the foregoing experimental and numerical studies have demonstrated that, for the $\Lambda = 50$ deg wing, at low angle of attack, a dual primary vortex system exists, whereas at higher angle of attack, this dual structure gives way to a single, larger-scale vortex that is a basic feature of highly swept wings.

Investigations at lower values of sweep angle include Yaniktepe and Rockwell,[8] who considered a wing of sweep angle $\Lambda = 38.7$ deg and addressed the flow structure well into the region of vortex breakdown via PIV. Yavuz et al.[9] investigated the near-surface topology and flow structure for a wing of sweep angle $\Lambda = 38.7$ deg, including the effect of wing perturbations and transient motion of the wing; a near-surface technique of PIV was employed.

For complex geometries such as an actual X-45 planform, both the fuselage and the wing extensions have low sweep angle. Elkhoury and Rockwell[10] and Elkhoury et al.[11] employed dye visualization in conjunction with PIV on cross-flow and near-surface planes to determine mean and unsteady representations of the flow structure.

B. Control of Flow Structure via Suction and Blowing

Different methods of control of the flow structure on a delta wing have been pursued to delay the onset of vortex breakdown, with the aim of reducing its undesired effects on the aerodynamic surface(s), as well as altering the overall performance characteristics of the planform. Suction and blowing in the tangential direction along the leading edge of a wing have been investigated by a number of researchers, with emphasis on highly swept wings. Wood et al.[12] and McCormick and Gursul[13] employed steady blowing and suction, whereas Gu et al.[14] applied periodic suction and blowing along the leading edge of the planform/wing. Intermittent trailing-edge blowing was studied by Vorobieff and Rockwell.[15] Parmenter and Rockwell[16] provided a different method, suction along the vortex axis at a location downstream of the onset of vortex breakdown, for delaying the onset of vortex breakdown. A unique approach to blowing is that of Johari et al.,[17] who provided blowing from surface ports oriented at different angles and located beneath the vortex core. Helin and Warty,[18] Shih and Ding,[19] Mitchell et al.,[20] and Phillips et al.[21] demonstrated the effect of trailing-edge blowing on the flow characteristics and onset of vortex breakdown. Further investigation on a closely related approach, which involved jet vectoring, was investigated by Wang et al.[22]

C. Unresolved Issues

Generally, very little effort has been devoted to control of the flow structure on wings having low sweep angle, which are representative of UCAV planforms. In particular, the following issues have not been addressed:

Received 4 March 2005; accepted for publication 8 September 2005.

*Research Assistant, Department of Mechanical Engineering and Mechanics.

†Paul B. Reinhold Professor, Department of Mechanical Engineering and Mechanics; dor0@lehigh.edu. Member AIAA.

1) The flow structure on delta wings of low sweep angle, in the absence of a control technique, should be defined in a systematic fashion, for example, by variations of angle of attack, with particular attention to the occurrence of vortex breakdown, surface buffeting, and stall, all interpreted in terms of quantitative representations of the surface flow topology, in particular classes of critical points. This approach can potentially lead to definition of a critical angle of attack at which the onset of three-dimensional separation occurs.

2) A particularly effective form of control may involve blowing at the trailing edge of a delta wing of low sweep angle. The anticipated onset of large-scale, three-dimensional surface separation and stall at relatively low angle of attack provides a flow state that may be sensitive to control by trailing-edge blowing. The minimum dimensionless blowing coefficient that yields a significant transformation of the near-surface flow structure and topology should be determined.

3) Trailing-edge blowing represents a form of control that is localized at the trailing edge, yet it may have a substantial global influence over the entire surface of the wing. Global alteration of the flow structure in the presence of localized control at a downstream location is a potentially important concept that may extend to other types of control approaches. Quantitative interpretation of patterns of the flow structure and topology at the wing surface can allow assessment of this concept.

4) Potential control of the mean (time-averaged) patterns of flow along the near surface of the wing is expected to have implications for surface buffeting phenomena, which can be represented in terms of patterns of velocity fluctuation amplitude along the surface. The interrelationship between the mean streamline topology (critical points) that indicate the onset of three-dimensional separation should be interpreted in terms of these patterns of fluctuation intensity.

This investigation aims to address these points using a technique of high-image-density PIV to characterize the flow patterns in the near-surface region of the wing.

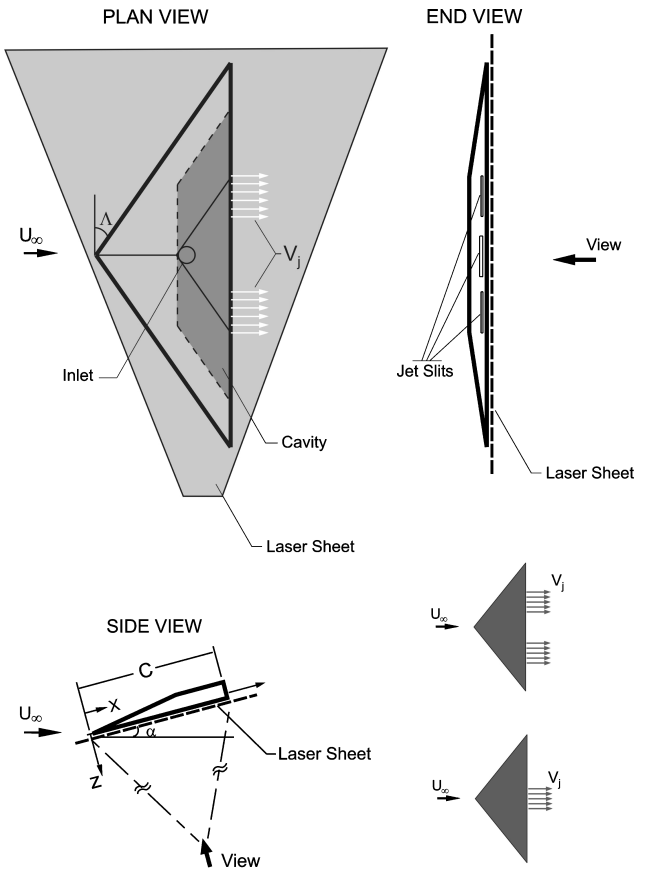

Fig. 1a Overview of experimental setup including delta wing and laser sheet orientation.

II. Experimental System and Techniques

Experiments were performed in a large-scale water channel, with a test section 927 mm wide, 610 mm deep, and 4928 mm long. This test section was preceded by a settling tank, a honeycomb screen arrangement, and a 2:1 contraction. The turbulence intensity at the entrance to the test section was less than 0.3%. The walls of this section were optically transparent. The free surface of the water was maintained at a height of 559 mm. The value of the Reynolds number Re based on chord C was maintained at 10^4. The corresponding value of freestream velocity was $U_\infty = 96.8$ mm/s.

The delta wing had a sweep angle of $\Lambda = 35$ deg, a chord C of 98 mm, and a total span at the trailing edge of 280 mm. The thickness of the wing was 12.7 mm, and its leading edges were beveled on the windward side at an angle of 15 deg. The angles of attack of the wing were $\alpha = 5$, 8, and 10 deg.

The inside of the delta wing was machined in the form of a cavity, in order to allow generation of uniform blowing from the trailing edge; this blowing is represented in the schematic of Fig. 1a. A water pump, control and bypass valves, and a volumetric flow meter were located outside of the water channel to generate, measure, and control the flow rate of the blowing. Two different configurations of trailing-edge blowing were used in the experiments: single and dual jets. For the single jet, the slit was located at midspan, that is, at the plane of symmetry of the wing. The width and the thickness of the slit were 25.4 and 1.6 mm, respectively. For the dual-jet system, the center of each slit was located 50.8 mm from the plane of symmetry of the wing. Each slit had width 25.4 mm and thickness 0.8 mm. For both single- and dual-jet configurations, seven different jet velocities were employed. These velocities corresponded to seven different momentum coefficients, $C_\mu = 0.006$, 0.025, 0.1, 0.23, 0.4, 0.92, and 1.63. The momentum coefficient was calculated as follows: $C_\mu = (V_j^2 \times A_j)/(U^2 \times A_s)$, in which V_j is the mean

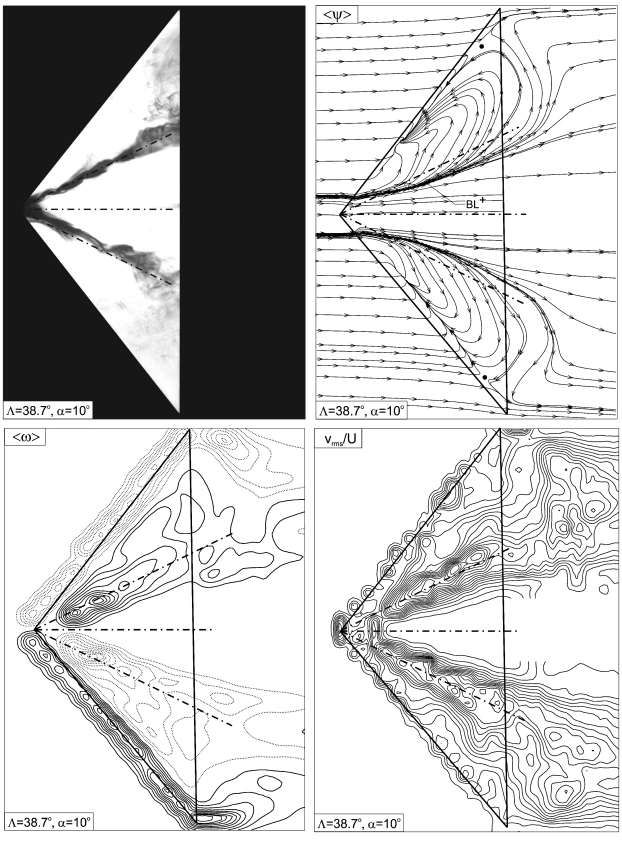

Fig. 1b Direct comparison of patterns of dye visualization, near-surface vorticity $\langle\omega\rangle$, root-mean-square of transverse velocity fluctuation v_{rms}/U, and streamline topology $\langle\Psi\rangle$ from Yavuz et al.[9] Sweep angle $\Lambda = 38.7$ deg, angle of attack $\alpha = 10$ deg, and Reynolds number $Re = 10^4$.

velocity of blowing at the trailing edge, A_j is the total area of both blowing slots the trailing edge, A_s is the surface area of the planform, and U is the freestream velocity. The wide range of momentum coefficients employed allowed examination of the possible regimes of response of the flow patterns induced by the trailing-edge blowing, taking into account values attainable in practical applications, as well as values employed in previous related investigations. Regarding previous studies, the maximum and minimum values given in the foregoing are comparable to those employed in the studies of Helin and Warty[18] and Shih and Ding.[19]

In this investigation, emphasis is on global patterns of the instantaneous flow structure, as well as cinema sequences of these patterns, which allow characterization of the timewise evolution of the flow and its time-averaged characteristics. A technique of high-image-density PIV was employed to generate quantitative flow patterns. The flow was seeded with 12-μm metallic-coated hollow plastic spheres. The seeding density of these particles was sufficiently large to satisfy the criterion of high image density; a minimum of 15 particle images were contained within the interrogation window. Illumination was provided by a dual-pulsed 90-mJ Nd: Yag laser system. The collinear beam was transmitted through a system of cylindrical and spherical lenses attached to the laser head in order to generate a laser sheet of thickness 1 mm. The maximum uncertainty of velocity was within 2%.

To obtain the near-surface flow patterns and topological characteristics, the laser sheet was located parallel and immediately adjacent to the surface of the wing, as shown in the plan and side views of Fig. 1a. For all images shown herein, the laser sheet had a thickness of 1 mm at the center of the wing, and its center of the sheet was located a distance of 1 mm from the surface of the wing. This location corresponds to a displacement z normal to the surface of the wing of $z/C = 0.01$, in which C is the root chord.

Patterns of particle images were recorded on a high-resolution digital charge-coupled device camera, having 1024×1024 pixels and an effective framing rate of 15 cycles per second. During evaluation of the velocity field V, a frame-to-frame cross-correlation technique was employed, with a 32×32 pixel interrogation window. The effective overlap was 50% to satisfy the Nyquist criterion. The spatial resolution of the flow field was optimized by acquiring images over half of the wing. Preliminary experiments, which involved a larger field of view, verified that the flow patterns induced by the trailing-edge blowing were symmetrical. The effective resolution, that is, grid size, was $\Delta/C = 0.0281$, 0.0286, and 0.0289 respectively for the angles of attack $\alpha = 5$, 8, and 10 deg.

Once the instantaneous velocity field V was determined, as described in the foregoing, it was possible to calculate time-averaged patterns of velocity $\langle V \rangle$, surface-normal vorticity $\langle \omega \rangle$, streamlines $\langle \Psi \rangle$, and root-mean-square transverse velocity fluctuation v_{rms}/U using the cinema sequence of images. To provide a guide for interpretation of these patterns, in relation to classical dye visualization, an excerpt from the investigation of Yavuz et al.[9] is given in Fig. 1b. It shows near-surface patterns for a wing of sweep angle similarly low that in the present study. For purposes of comparison, reference lines are superposed on each image; they are coincident with the centerline of the dye-visualized vortex cores. These lines pass through the extrema of the surface-normal vorticity $\langle \omega \rangle$ contours, thereby indicating that patterns of $\langle \omega \rangle$ serve as a near-surface footprint of the leading-edge vortex. Patterns of $\langle \Psi \rangle$ show positive bifurcation lines BL^+, which represent lines of attachment, and according to the aforementioned reference lines the vortex cores lie outboard of the attachment lines. Again using reference lines as a guide, extrema of root-mean-square velocity fluctuation v_{rms}/U satisfy two conditions: they are located beneath the unsteady vortex core, and they are close to the attachment line, which represents the approximate location of reattachment of the shear layer emanating from the leading edge of the wing. In fact, Taylor and Gursul[7] and Elkhoury et al.,[11] in investigations that observed the leading-edge vortex and its breakdown on wings of low sweep angle, related reattachment of the separated shear layer from the windward side of the wing to the wing surface and the relatively large magnitudes of near-surface fluctuations in the region of reattachment. The foregoing interrelationships can aid in interpretation of the images addressed herein, which show the effects of trailing-edge blowing on the near-surface patterns.

III. Near-Surface Topology in Absence of Control: Effect of Angle of Attack

Figure 2 shows patterns of time-averaged velocity vectors $\langle V \rangle$ (left column) and streamlines $\langle \Psi \rangle$ (right column) in the absence of trailing-edge blowing for angles of attack $\alpha = 5$, 8, and 10 deg. At all values of α, the magnitude of $\langle V \rangle$ shows an abrupt decrease immediately downstream of the leading-edge. As the value of α increases from $\alpha = 5$ deg to $\alpha = 10$ deg, the spatial extent of the region of very low velocity increases. Furthermore, at $\alpha = 8$ deg, the onset of a well-defined swirl pattern of velocity is evident in the region near the apex, and at $\alpha = 10$ deg, this swirl pattern has a larger extent and is particularly well defined. Within the central portion of each of these swirl patterns of $\alpha = 8$ and 10 deg, the magnitude of $\langle V \rangle$ is very small.

The corresponding patterns of streamline $\langle \Psi \rangle$ topology, shown in the right-hand column of Fig. 2, have well-defined features, which can be characterized in terms of critical points. At $\alpha = 5$ deg, a negative bifurcation line BL^- extends over a substantial extent of the leading edge. It corresponds to the merging of streamlines toward a single line, and represents a line of separation. In the vicinity of the apex, BL^- terminates in the node N_1, to which streamlines tend to converge. In the outboard region of the wing, a saddle point S_1 is evident; it represents the apparent intersection of streamlines. Furthermore, a positive bifurcation line BL^+, which is a line from which streamlines tend to diverge, is evident; it represents a line of

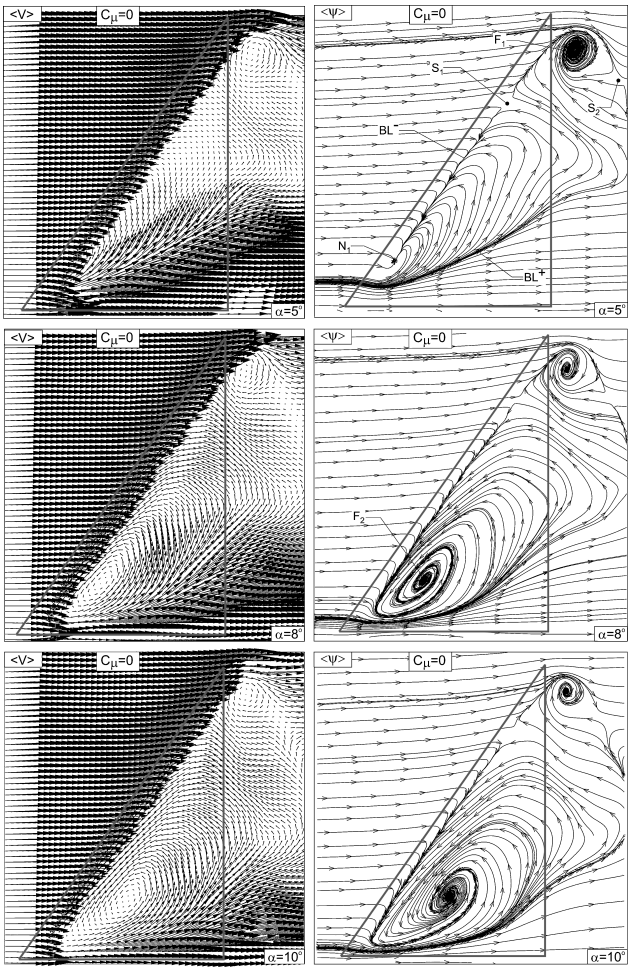

Fig. 2 Near-surface flow patterns of time-averaged velocity $\langle V \rangle$ and streamlines $\langle \Psi \rangle$ on wings at different angles of attack $\alpha = 5$, 8, and 10 deg.

attachment. In addition, a well-defined focus F_1, which represents the center of an inward swirl pattern of streamlines, occurs immediately downstream of the tip of the wing. An additional saddle point S_2 is also apparent in this region.

At the higher angle of attack $\alpha = 8$ deg in Fig. 2, the node N_1 gives way to a large-scale focus F_2. It has been observed experimentally in surface skin friction visualization, near-surface streamlines, and numerical simulations on a variety of planar surfaces, bodies and wings by Legendre,[23] Perry and Hornung,[24] Perry and Chong,[25] Dallman and Schulte-Werning,[26] Su et al.,[27] Lazos,[28] and Taylor and Gursul.[7] All of these investigations show an inward-spiraling surface streamline pattern that culminates in a stable focus. The relationship between this focus at the surface and the flow away from the surface, in particular the development of a three-dimensional vortical structure, has been quantitatively described by Perry and Hornung,[24] Perry and Chong,[25] and Dallman and Schulte-Werning.[26] Here, existence of the focus F_2 will be taken as an indicator of three-dimensional separation, with the realization that the initial onset of separation may occur at, for example, a critical point located immediately upstream of the focus.

It is interesting to note that despite the onset of the large-scale focus F_2, all of the other critical points, that is, BL^-, S_1, BL^+, F_1, and S_2, are still identifiable. A further increase to $\alpha = 10$ deg yields a still larger-scale inward-swirling pattern of streamlines, which culminates in the focus F_2; it is located farther downstream than the F_2 at $\alpha = 8$ deg. Again, at $a = 10$ deg, all other critical points are still detectable.

Figure 3 (left-hand column) shows patterns of time-averaged, surface-normal vorticity $\langle\omega\rangle$, whereby the orientation of positive vorticity is in the direction of the outward surface normal. Dashed and solid lines indicate respectively negative and positive values of $\langle\omega\rangle$. Along the leading edge of the wing, well-defined clusters of negative $\langle\omega\rangle$ occur, due to a three-dimensional instability of the shear layer separating from the windward surface of the wing. Regarding the positive, elongated layer of vorticity at $\alpha = 5$ deg, its form is generally similar to that characterized by Yavuz et al.[9] for a wing of different but low sweep angle. Corresponding dye visualization showed that this well-defined region of vorticity is the footprint of the leading-edge vortex, as represented in Fig. 1b. At $\alpha = 8$ and 10 deg, however, the elongated layer of vorticity moves dramatically closer to the plane of symmetry of the wing and becomes narrower in extent. These patterns suggest that the locus of the vortex emanating from the apex of the wing is close to the plane of symmetry of the wing. In fact, dye visualization (in the absence of surface patterns) of Yaniktepe and Rockwell[8] show that, at sufficiently high angle of attack, the visualized vortex moves from a well-defined leading-edge vortex to a vortex close to the plane of symmetry of the wing.

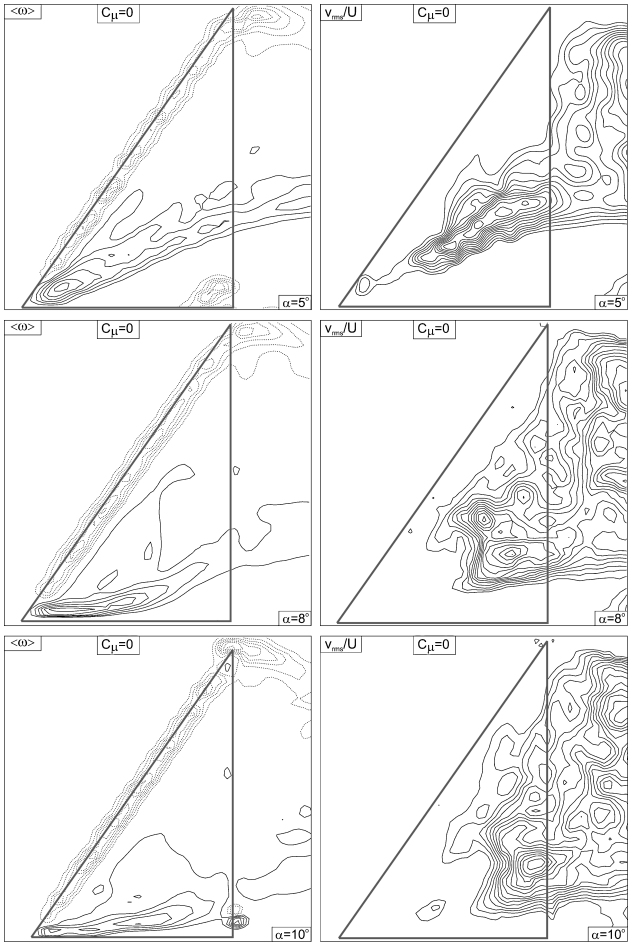

Fig. 3 Patterns of time-averaged vorticity $\langle\omega\rangle$ oriented in a direction normal to the surface of the wing and root-mean-square of transverse velocity fluctuation v_{rms}/U on wings at different angles of attack $\alpha = 5$, 8, and 10 deg: $[|\langle\omega\rangle|]_{min} = 2\ s^{-1}$, $\Delta[|\langle\omega\rangle|] = 2\ s^{-1}$, $[v_{rms}/U]_{min} = 0.05$, $\Delta[v_{rms}/U] = 0.01$.

Figure 3 (right-hand column) provides contours of constant root-mean-square velocity transverse fluctuation v_{rms}/U as a function of angle of attack α. Consider first $\alpha = 5$ deg. The relation between the visualized leading-edge vortex, the v_{rms}/U contours, the surface-normal vorticity $\langle\omega\rangle$, and the streamlines $\langle\Psi\rangle$ on a wing of similarly low sweep angle is given in Fig. 1b, based on images of Yavuz et al.[9] The type of v_{rms}/U contour distribution given at $\alpha = 5$ deg in Fig. 3 is coincident with the footprint of the leading-edge vortex, which has undergone breakdown (compare Fig. 1b), and close to the line of attachment. At higher values of $\alpha = 8$ and 10 deg, where the large-scale focus forms, the patterns of v_{rms}/U are dramatically broadened and, at the higher value of $\alpha = 10$ deg, the peak values of v_{rms}/U are located closer to the trailing edge than at $\alpha = 8$ deg. These much broader patterns of v_{rms}/U occur in accord with the onset of the large-scale swirl pattern of streamlines and the focus F_2 shown in the right column of Fig. 2.

Viewing together the patterns of Figs. 2 and 3, onset of a large-scale inward-spiral pattern culminating in the focus F_2 dramatically affects the topology between the positive and negative bifurcation lines BL^- and BL^+. Remarkably, however, other critical points on the planform and in its wake remain relatively unchanged. This major transformation of the near-surface topology is associated with similarly radical transformations of the pattern of $\langle\omega\rangle$, which, at sufficiently low angle of attack, represents the footprint of the vortex, as well as patterns of near-surface velocity fluctuation v_{rms}/U.

IV. Near-Surface Topology: Effect of Trailing-Edge Blowing

The near-surface flow patterns on the wing of low sweep angle, at angles of attack $\alpha = 5$, 8, and 10 deg, are shown in Figs. 4–9 for a range of dimensionless blowing coefficients extending from $C_\mu = 0.006$ to 1.63. This coefficient C_μ is defined in Sec. II. Further values of C_μ were considered within the aforementioned range in order to allow generalization of the observations.

A. Patterns Below Critical Angle of Attack

Figures 4 and 5 show patterns of streamline $\langle\Psi\rangle$ topology, surface-normal vorticity $\langle\omega\rangle$, and root-mean-square of near-surface velocity fluctuation v_{rms}/U at an angle of attack $\alpha = 5$ deg, which, in accord with the reference patterns of Figs. 2 and 3, lies below the critical angle of attack.

The patterns of $\langle\Psi\rangle$ of Fig. 4 show that, up to a value of $C_\mu = 0.025$, the location and form of the nodal point N_1, the negative bifurcation line BL^-, the saddle point S_1, and the focal point F_1 remain relatively the same, in both location and form, as for the case of no blowing $C_\mu = 0$. In the region bounded by the negative bifurcation line BL^- and the positive line BL^+, however, substantial changes in the form of the streamline pattern occur, even for the lowest value of $C_\mu = 0.006$.

At $C_\mu = 0.1$, the overall pattern of $\langle\Psi\rangle$ starts to undergo a fundamental change, and at $C_\mu = 0.4$, it is fundamentally different. The node N_1 and the saddle point S_1 have disappeared in favor of a nodal point N_2, which is accompanied by movement of the saddle point

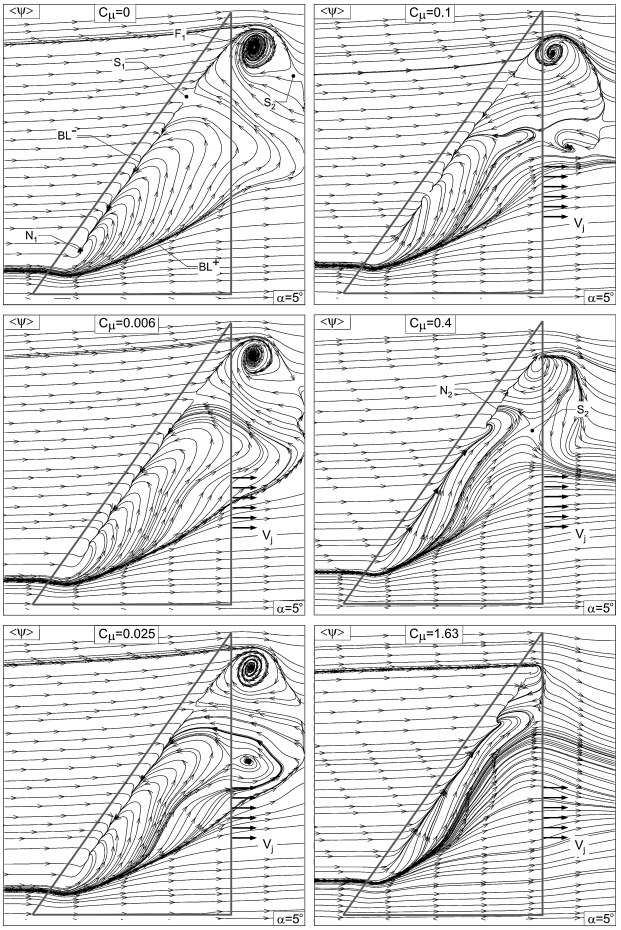

Fig. 4 Comparison of near-surface patterns of time-averaged streamlines $\langle\Psi\rangle$ for dual blowing cases for momentum coefficients $C_\mu = 0$, 0.006, 0.025, 0.1, 0.4, and 1.63 on a wing at angle of attack $\alpha = 5$ deg. $C_\mu = (V_j^2 \times A_j)/(U^2 \times A_s)$, in which V_j is the mean velocity of blowing at the trailing edge, A_j is the total area of both blowing slots at the trailing edge, A_s is the surface area of the planform, and U is the freestream velocity.

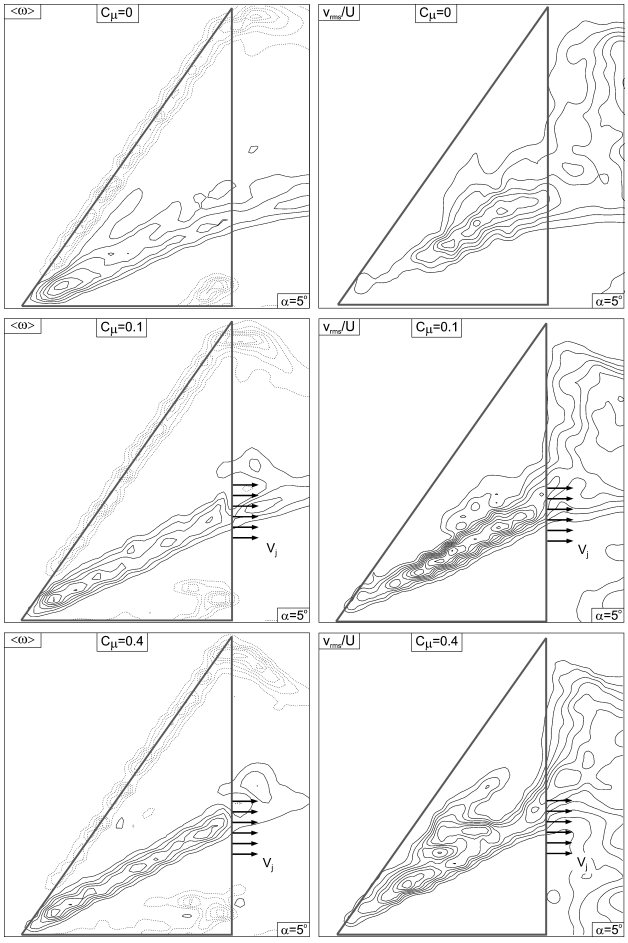

Fig. 5 Comparison of vorticity $\langle\omega\rangle$ oriented in a direction normal to the surface of the wing and root-mean-square of transverse velocity fluctuation $v_{\rm rms}/U$ for dual-location blowing cases for momentum coefficients $C_\mu = 0$, 0.1, and 0.4 on a wing at angle of attack $\alpha = 5$ deg. $C_\mu = (V_j^2 \times A_j)/(U^2 \times A_s)$, in which V_j is the mean velocity of blowing at the trailing edge, A_j is the total area of both blowing slots at the trailing edge, A_s is the surface area of the planform, and U is the freestream velocity: $[|\langle\omega\rangle|]_{\rm min} = 2\ {\rm s}^{-1}$, $\Delta[|\langle\omega\rangle|] = 2\ {\rm s}^{-1}$, $[v_{\rm rms}/U]_{\rm min} = 0.05$, $\Delta[v_{\rm rms}/U] = 0.02$.

S_2 to a location immediately upstream of the trailing edge of the wing. It is therefore evident that, at sufficiently large C_μ, there is a reduction of the number of critical points along the leading edge of the wing, and, simultaneously, movement of the saddle point S_2 from the wake region to a location on the surface of the wing.

A still further change of the pattern of $\langle\Psi\rangle$ at relatively high values of C_μ is the decreasing distance between the negative bifurcation line BL^- along the leading-edge of the wing and the positive bifurcation line BL^+. At values of $C_\mu = 0.4$ and 1.63, they nearly become coincident. Simultaneously, the focus F_2, which is evident at a location close to the tip of the wing for lower values of C_μ, disappears at these higher values.

Figure 5 (left-hand column) shows patterns of surface normal vorticity $\langle\omega\rangle$ at two selected values of blowing coefficient in relation to the case of no blowing. At $C_\mu = 0$, a single, well-defined peak (extremum) of $\langle\omega\rangle$ occurs near the apex, and for larger values of $C_\mu = 0.1$ and 0.4, multiple peaks occur over the entire elongated distribution of $\langle\omega\rangle$. The onset of these multiple peaks corresponds to substantial changes of the patterns of instantaneous ω, not shown here, and thereby occurrence of substantial unsteadiness. A further feature of the elongated patterns of $\langle\omega\rangle$ is that the angle of inclination of the pattern with respect to the plane of symmetry of the wing increases with increasing C_μ.

Figure 5 (right-hand column) shows patterns of $v_{\rm rms}/U$. At $C_\mu = 0.1$, peak values of $v_{\rm rms}/U$ are significantly larger and appear closer to the apex of the wing than the patterns at $C_\mu = 0$. Furthermore, at $C_\mu = 0.4$, even larger magnitudes of $v_{\rm rms}/U$ occur closer to the apex. As was the case for the patterns of $\langle\omega\rangle$, the angle of inclination of the elongated pattern of $v_{\rm rms}/U$ with respect to the plane of symmetry of the wing increases with increasing C_μ.

The patterns of both $\langle\omega\rangle$ and $v_{\rm rms}/U$ at $C_\mu = 0.1$ and 0.4 in Fig. 5 can be directly compared with the corresponding patterns of streamline $\langle\Psi\rangle$ topology in Fig. 4. At these two values of C_μ, the positive bifurcation line BL^+ is in the process of transformation, whereby the line BL^+ present at $C_\mu = 0$ undergoes substantial broadening. This transformation of the $\langle\Psi\rangle$ is therefore associated with enhanced unsteadiness and deflection of the pattern of $v_{\rm rms}/U$, which is thereby consistent with deflection of the new line of reattachment, that is, the new location of BL^+ away from the plane of symmetry of the wing.

B. Patterns Above Critical Angle of Attack

The onset of a well-defined focus, and thereby a region of three-dimensional separation, occurs at an angle of attack above a critical value, as defined in the overview of Fig. 2. Figure 6 shows the consequence of trailing-edge blowing in this regime for an angle of attack $\alpha = 8$ deg. For the reference case, $C_\mu = 0$, the topology indicates negative and positive bifurcation lines BL^- and BL^+, which represent lines of separation and attachment; saddle points S_1 and S_2; and focal points F_1 and F_2.

Even for a very small value of blowing coefficient $C_\mu = 0.006$ in Fig. 6, the location of the focus F_2 is displaced closer to the apex of the wing and, furthermore, detectable changes in the pattern of streamlines occurs in the region between the negative and positive bifurcation lines BL^- and BL^+. When $C_\mu = 0.025$, the focus F_2

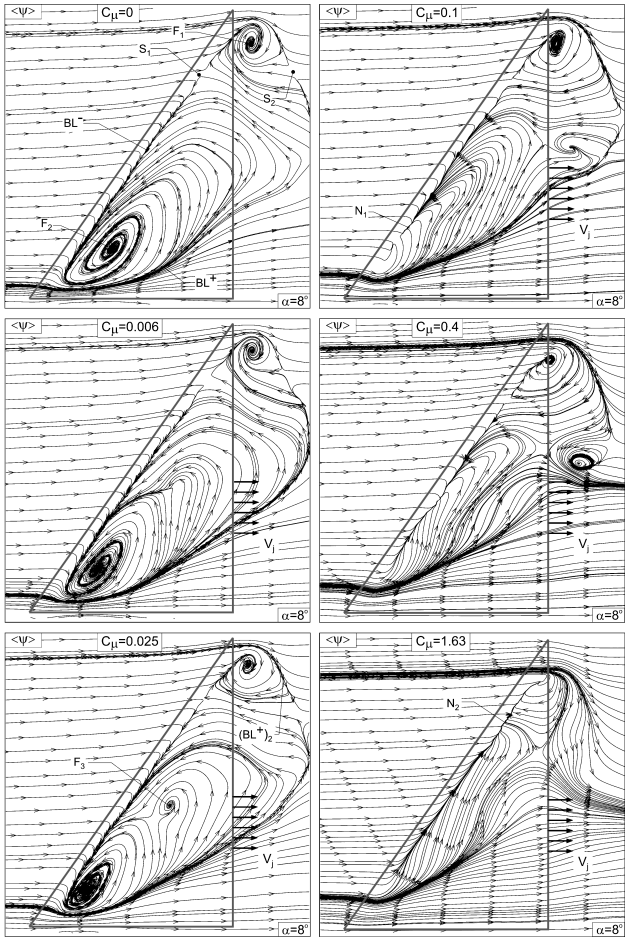

Fig. 6 Comparison of near-surface patterns of time-averaged streamlines $\langle\Psi\rangle$ for dual blowing cases for momentum coefficients $C_\mu = 0$, 0.006, 0.025, 0.1, 0.4, and 1.63 on a wing at angle of attack $\alpha = 8$ deg. $C_\mu = (V_j^2 \times A_j)/(U^2 \times A_s)$, in which V_j is the mean velocity of blowing at the trailing edge, A_j is the total area of both blowing slots at the trailing edge, A_s is the surface area of the planform, and U is the freestream velocity.

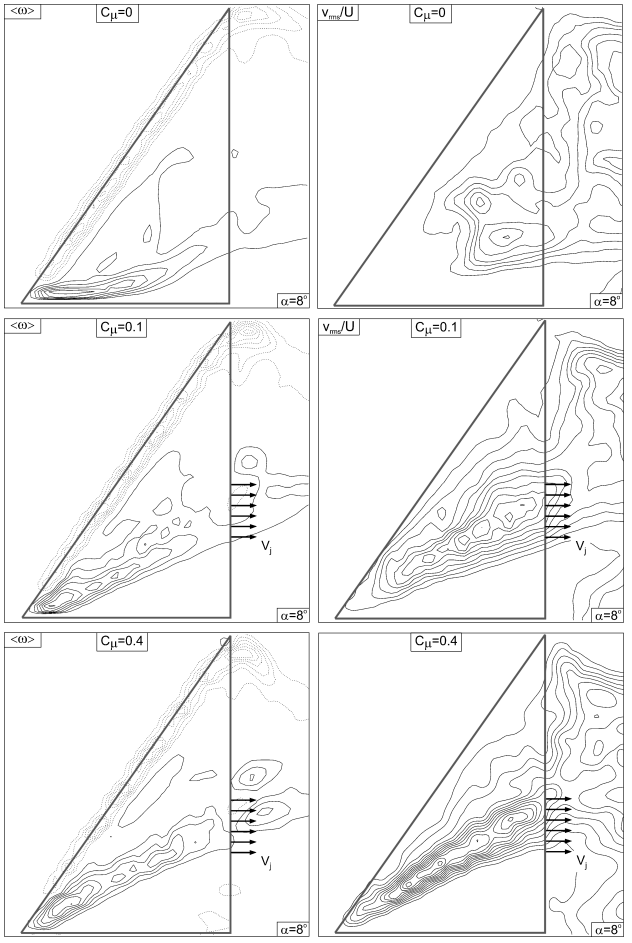

Fig. 7 Comparison of vorticity $\langle\omega\rangle$ oriented in a direction normal to the surface of the wing and root-mean-square of transverse velocity fluctuation $v_{\rm rms}/U$ for dual-location blowing cases for momentum coefficients $C_\mu = 0$, 0.1, and 0.4 on a wing at angle of attack $\alpha = 8$ deg. $C_\mu = (V_j^2 \times A_j)/(U^2 \times A_s)$, in which V_j is the mean velocity of blowing at the trailing edge, A_j is the total area of both blowing slots at the trailing edge, A_s is the surface area of the planform, and U is the freestream velocity: $[|\langle\omega\rangle|]_{\rm min} = 2\ {\rm s}^{-1}$, $\Delta[|\langle\omega\rangle|] = 2\ {\rm s}^{-1}$, $[v_{\rm rms}/U]_{\rm min} = 0.05$, $\Delta[v_{\rm rms}/U] = 0.02$.

moves even closer to the apex of the wing and, furthermore, a small-scale focus F_3 occurs. Remarkable is the fact that, although these topological changes are occurring at locations upstream of the trailing edge of the wing for $C_\mu = 0.006$ and 0.025, the alteration of the patterns downstream of the trailing edge is relatively insignificant. Furthermore, a secondary positive bifurcation line designated as $(BL^+)_2$, which is detectable at lower values of C_μ, becomes clearly evident near the tip of the wing in the image at $C_\mu = 0.025$, and at larger values of C_μ as well.

Increase of the blowing coefficient to a value of $C_\mu = 0.1$ in the series of Fig. 6 has the striking effect of eradicating the focus F_2. That is, the occurrence of a large-scale swirl pattern of streamlines no longer exists; rather, it is replaced by the nodal point N_1. In this respect, the topology is very similar to the topology at the lower angle of attack $\alpha = 5$ deg in the absence of blowing, as indicated in Fig. 4.

At still higher values of $C_\mu = 0.4$ and 1.63 in Fig. 6, the transformation of the topology is similar to that occurring in Fig. 4. More specifically, in Fig. 6, at $C_\mu = 1.63$, the nodal point N_1 and the saddle point S_1 have disappeared in favor of the single nodal point N_2. Simultaneously, the positive bifurcation line $(BL^+)_2$ becomes more diffuse at $C_\mu = 1.63$. [The line $(BL^+)_2$ is designated at the tip of the wing at $C_\mu = 0.025$.]

Figure 7 (left-hand column) shows patterns of surface normal vorticity $\langle\omega\rangle$ at representative values of blowing coefficient C_μ. As it is increased to $C_\mu = 0.1$, and then to 0.4, it is evident that the pattern of vorticity transforms to a well-defined, elongated form that is characteristic of the wing at lower angle of attack in the absence of blowing (compare pattern of $\langle\omega\rangle$ at $C_\mu = 0$ in Fig. 3). This process corresponds to reestablishment of the well-defined leading-edge vortex; Yavuz et al.[9] have shown that the type of pattern of $\langle\omega\rangle$ at $C_\mu = 0.4$ is the footprint of the dye vortex visualized above the wing at sufficiently low angle of attack. Direct comparison of patterns of $\langle\omega\rangle$ at $C_\mu = 0.1$ and 0.4 with the corresponding patterns of $\langle\Psi\rangle$ in Fig. 6 shows that they correspond to disappearance of the focus F_2 associated with large-scale separation.

Figure 7 (right-hand column) shows the patterns of $v_{\rm rms}/U$. These near-surface patterns, which are an indication of the buffet loading, undergo a transformation in accord with the aforementioned patterns of $\langle\omega\rangle$ and $\langle\Psi\rangle$. At $C_\mu = 0$, where large-scale separation exists over the surface of the wing, the pattern of $v_{\rm rms}/U$ is broadly distributed. In the presence of blowing at $C_\mu = 0.1$, the pattern of $v_{\rm rms}/U$ starts to take on an elongated form, and the peak values become somewhat higher. In fact, even for lower values of $C_\mu = 0.006$ and 0.025 (not shown), significant upstream movement of the peak values of $v_{\rm rms}/U$ is evident. At $C_\mu = 0.4$, the pattern of $v_{\rm rms}/U$ is sharply defined and relatively narrow. Furthermore, the peak values have increased substantially. Thus, we have the remarkable observation that eradication of separation over a substantial portion of the wing surface via trailing-edge blowing, which is associated with reestablishment of a well-defined leading-edge vortex, actually results in higher near-surface fluctuation amplitudes over a narrowly defined region. In fact, these regions of high fluctuation are close to the primary (positive) bifurcation line BL^+, that is, the attachment line.

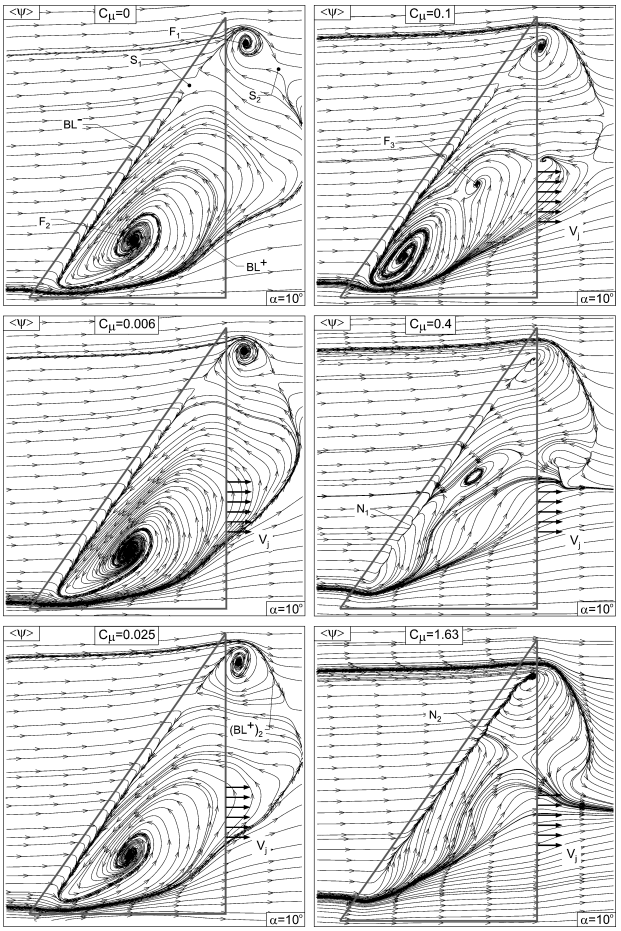

Fig. 8 Comparison of near-surface patterns of time-averaged streamlines $\langle\Psi\rangle$ for dual blowing cases for momentum coefficients $C_\mu = 0$, 0.006, 0.025, 0.1, 0.4, and 1.63 on a wing at angle of attack $\alpha = 10$ deg. $C_\mu = (V_j^2 \times A_j)/(U^2 \times A_s)$, in which V_j is the mean velocity of blowing at the trailing edge, A_j is the total area of both blowing slots at the trailing edge, A_s is the surface area of the planform, and U is the freestream velocity.

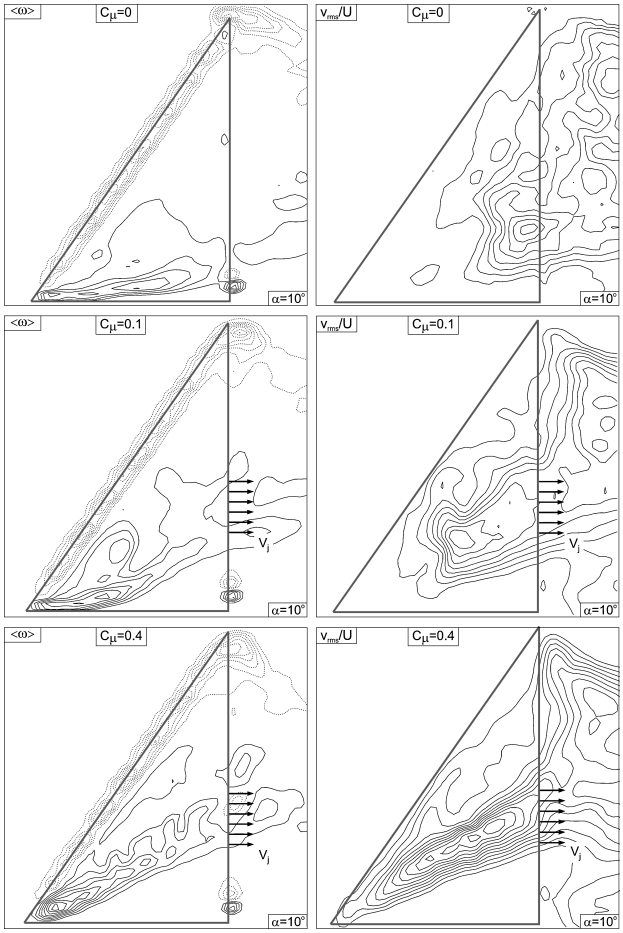

Fig. 9 Comparison of vorticity $\langle\omega\rangle$ oriented in a direction normal to the surface of the wing and root-mean-square of transverse velocity fluctuation $v_{\rm rms}/U$ for dual-location blowing cases for momentum coefficients $C_\mu = 0$, 0.1, and 0.4 on a wing at angle of attack $\alpha = 10$ deg. $C_\mu = (V_j^2 \times A_j)/(U^2 \times A_s)$, in which V_j is the mean velocity of blowing at the trailing edge, A_j is the total area of both blowing slots at the trailing edge, A_s is the surface area of the planform, and U is the freestream velocity: $[|\langle\omega\rangle|]_{\rm min} = 2\ {\rm s}^{-1}$, $\Delta[|\langle\omega\rangle|] = 2\ {\rm s}^{-1}$, $[v_{\rm rms}/U]_{\rm min} = 0.05$, $\Delta[v_{\rm rms}/U] = 0.02$.

At a higher angle of attack, as shown in Fig. 8, the patterns of streamline $\langle\Psi\rangle$ topology undergo a transformation during increases of C_μ generally similar to that for angle of attack $\alpha = 8$ deg. The disappearance of the focus F_2 at a sufficiently high value of $C_\mu = 0.4$ is the predominant change. It appears that a higher value of $C_\mu = 0.4$ is required to eradicate the focus F_2 involving three-dimensional separation, relative to the case of the lower angle of attack $\alpha = 8$ deg; as shown in Fig. 6, the focus F_2 could be eradicated at $C_\mu = 0.1$. Note also that a small-scale focus at F_3 appears at $C_\mu = 0.1$. This type of focus was also evident at $\alpha = 8$ deg, but at a substantially lower value of blowing coefficient $C_\mu = 0.025$, as indicated in Fig. 6.

Furthermore, Fig. 9 shows patterns of $\langle\omega\rangle$ and $v_{\rm rms}/U$, which follow a trend generally similar to that at $\alpha = 8$ deg in Fig. 7. The pattern of $\langle\omega\rangle$ transforms, at a sufficiently high value of $C_\mu = 0.4$, to a general form characteristic of a footprint of a well-defined leading-edge vortex. The patterns of $v_{\rm rms}/U$ are generally similar at $C_\mu = 0$, but the peak value is close to the trailing edge at $\alpha = 10$ deg in Fig. 9, relative to peak values occurring upstream of the trailing edge at $\alpha = 8$ deg in Fig. 7. Furthermore, at $\alpha = 10$ deg, the pattern of $v_{\rm rms}/U$ remains relatively broadly distributed, whereas at $\alpha = 8$ deg, $C_\mu = 0.1$ in Fig. 7, it has already taken the general form of an elongated distribution. At $C_\mu = 0.4$, $\alpha = 10$ deg in Fig. 9, the pattern of $v_{\rm rms}/U$ has a very well-defined elongated form with high fluctuation level, very similar to that of the same value of C_μ at $\alpha = 8$ deg shown in Fig. 7.

Viewing together the near-surface patterns above the critical angle of attack, that is, at $\alpha = 8$ and 10 deg, shown in Figs. 6–9, the transformations of the near-surface topology with increasing values of blowing coefficient C_μ are remarkably similar. Larger values of C_μ are required, however, to induce the topological change at the higher $\alpha = 10$ deg, relative to $\alpha = 8$ deg. Nevertheless, the remarkable similarities of the transformed patterns indicate that they are robust, which is further evident by examining the types and locations of the critical points of the topology. In other words, despite the fact that the patterns at $\alpha = 10$ deg are less sensitive to this trailing-edge control technique, the topology follows the same sequence of alterations, or transformations, as at lower angle of attack at $\alpha = 8$ deg. Similar statements can be made for the patterns of surface-normal vorticity $\langle\omega\rangle$ and near-surface velocity fluctuation $v_{\rm rms}/U$; that is, similar types of transformations are evident with increasing C_μ.

V. Near-Surface Patterns: Comparison of Dual and Single Trailing-Edge Blowing

To determine the sensitivity of the near-surface patterns to location of the blowing slot, the case of a single jet aligned with the plane of symmetry of the wing is compared with the dual jet, which has been the focus of the preceding sections. Figure 10 provides this comparison for two values of blowing coefficient: $C_\mu = 0.1$ and 1.63. For the case of the single jet, at $C_\mu = 0.1$, the pattern of streamline $\langle\Psi\rangle$ topology is essentially the same as that in the absence of blowing (compare Fig. 2), except that the location of the focus F_2 is shifted slightly upstream and a secondary positive bifurcation line $(BL^+)_2$ becomes apparent. On the other hand, for the case of the dual jet at $C_\mu = 0.1$, the pattern of surface topology is fundamentally

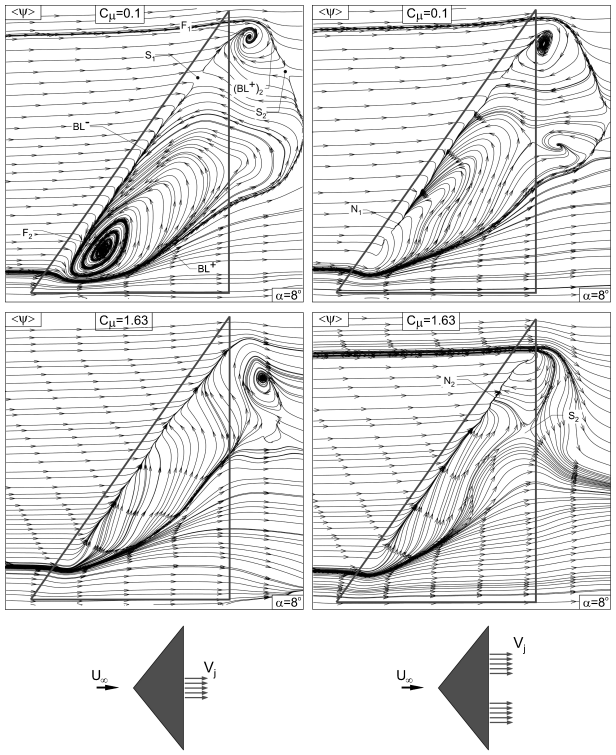

Fig. 10 Comparison of near-surface patterns of time-averaged streamlines $\langle\Psi\rangle$ for single-blowing and dual-blowing cases for momentum coefficients $C_\mu = 0.1$ and 1.63 on a wing at angle of attack $\alpha = 8$ deg. $C_\mu = (V_j^2 \times A_j)/(U^2 \times A_s)$, in which V_j is the mean velocity of blowing at the trailing edge, A_j is the total area of both blowing slots at the trailing edge, A_s is the surface area of the planform, and U is the freestream velocity.

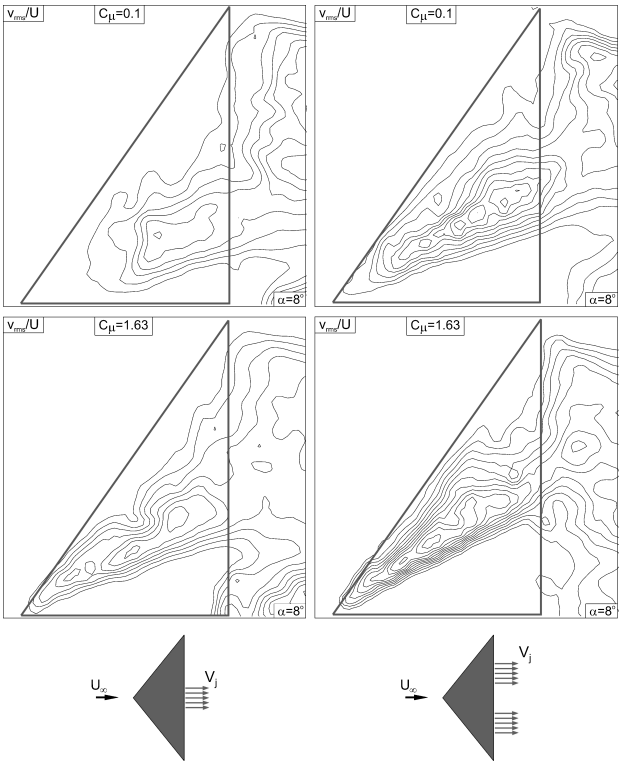

Fig. 11 Comparison of root-mean-square of transverse velocity fluctuation $v_{\rm rms}/U$ for single-blowing and dual-blowing cases for momentum coefficients $C_\mu = 0.1$ and 1.63 on a wing at angle of attack $\alpha = 8$ deg. $C_\mu = (V_j^2 \times A_j)/(U^2 \times A_s)$, in which V_j is the mean velocity of blowing at the trailing edge, A_j is the total area of both blowing slots at the trailing edge, A_s is the surface area of the planform, and U is the freestream velocity: $[v_{\rm rms}/U]_{\rm min} = 0.05$, $\Delta[v_{\rm rms}/U] = 0.02$.

transformed; that is, the focus F_2 and thereby the region of large-scale separation are eradicated, as demonstrated in Fig. 6.

If the magnitude of the blowing coefficient is increased to a relatively high value of $C_\mu = 1.63$ for the case of the single jet, however, the pattern of $\langle\Psi\rangle$ is as indicated in Fig. 10; that is, the focus F_2 and secondary positive bifurcation line $(BL^+)_2$ are now eradicated. Furthermore, aside from the negative and positive bifurcation lines BL^- and BL^+, no other critical features exist along the surface of the wing. All the critical points on the surface of the wing are eradicated. On the other hand, for the case of the dual jet with blowing at $C_\mu = 1.63$, a node N_2 and a saddle point S_2 remain on the wing surface, in addition to the negative and positive bifurcation lines, BL^- and BL^+. In addition, for this case, the secondary positive bifurcation line $(BL^+)_2$ remains and has become diffuse. Thus, remarkably, the single jet yields a much simplified $\langle\Psi\rangle$ topology relative to the case of the dual jet at a relatively high value of blowing coefficient C_μ. Furthermore, for the case of the dual jet, the bifurcation line BL^+ is relatively diffused, relative to the well-defined line BL^+ for the case of the single jet at $C_\mu = 1.63$; in this case, it persists in a well-defined fashion to the trailing edge of the wing.

Figure 11 shows contours of constant $v_{\rm rms}/U$, which correspond to the $\langle\Psi\rangle$ topology patterns of Fig. 10. At the low value of blowing coefficient $C_\mu = 0.1$, the pattern of $v_{\rm rms}/U$ for the single jet is relatively broadly distributed and has low peak values; this observation is in accord with the existence of the focus F_2 shown in Fig. 10, and thereby the occurrence of three-dimensional separation. On the other hand, for the case of the dual jet at $C_\mu = 0.1$, the peak values of fluctuation are significantly larger, and the overall pattern of $v_{\rm rms}/U$ tends to take an elongated form. This higher level and more ordered form are associated with eradication of the focus F_2 and thereby the region of large-scale separation, designated in Fig. 10. At larger values of blowing coefficient $C_\mu = 1.63$, both the single jet and dual jet yield relatively elongated and ordered patterns of $v_{\rm rms}/U$, but significantly higher values occur for the dual jet. Taking an overview of all of the patterns in Fig. 11, it appears that the single jet tends to induce lower values of near-surface velocity fluctuation $v_{\rm rms}/U$, relative to the dual jet.

VI. Conclusions

The near-surface patterns on a delta wing at low sweep angle have been investigated as a function of both angle of attack and magnitude of localized blowing from slots at the trailing edge. Patterns of streamline topology, involving several classes of critical points, surface-normal vorticity, and root-mean-square velocity fluctuations allow quantitative representation of the sensitivity of the patterns to magnitude of the blowing coefficient. The principal findings are as follows:

1) For the reference case of no blowing from the trailing edge, there exists a critical value of angle of attack, above which large-scale, three-dimensional surface separation occurs. It is defined by a stable focus, that is, center of an inward-spiraling pattern located immediately downstream of the apex of the wing. When this regime occurs, the pattern of near-surface velocity fluctuation has a substantially larger spatial extent, with peak amplitudes that are shifted toward the trailing edge of the wing.

2) At an angle of attack lower than the critical value, application of trailing-edge blowing, even at a very small magnitude, can significantly alter the topological pattern between the lines of separation and attachment. When the magnitude of the blowing coefficient is sufficiently large, the nature and location of the critical points of the near-surface streamline topology are fundamentally altered, both along the surface of the wing and in its near wake.

3) Above the critical angle of attack, the major consequence of trailing-edge blowing is to move the focus of the inward-spiraling streamline pattern, which represents the locus of three-dimensional separation, toward the apex of the wing, and when the value of the blowing coefficient reaches a critical value, this focus is entirely eliminated. This change in near-surface topology is accompanied

by recovery of patterns of surface-normal vorticity and root-mean-square near-surface velocity fluctuations that are characteristic of a well-defined vortex above the surface of the wing. That is, the patterns of root-mean-square velocity fluctuation transform from broadly distributed, lower-level contours to highly concentrated, relatively high-level contours of fluctuation magnitude. The consequence of trailing-edge blowing is therefore to transform the patterns to forms very similar to those at lower angle of attack in the absence of trailing-edge blowing.

4) When the angle of attack is significantly higher than the critical value, the near-surface patterns are generally less sensitive to trailing-edge blowing. Nevertheless, the transformation between successive states of near-surface streamline topology, surface-normal vorticity, and root-mean-square velocity fluctuation follow the same sequence and form as for lower angle of attack; larger values of blowing coefficient are, however, required to induce these states of the flow.

5) Comparison of blowing from a single slot centered at the plane of symmetry of the wing with the foregoing cases of dual blowing indicates that, at lower values of blowing coefficient, the dual blowing configuration induces radical changes in the near-surface pattern, whereas the single jet induces almost no change. On the other hand, when the blowing coefficient becomes sufficiently large, the single blowing jet is remarkable effective, and it minimizes the number of critical features occurring on the surface of the wing, relative to the case of dual jet blowing.

Acknowledgments

The support of the Air Force Office of Scientific Research (AFOSR) under Grant F49620-02-1-0061 is gratefully acknowledged. This AFOSR program was monitored by John Schmisseur.

References

[1]Ol, M. V., and Gharib, M., "The Passage Towards Stall of Nonslender Delta Wings at Low Reynolds Number," AIAA Paper 2001-2843, June 2001.

[2]Ol, M. V., and Gharib, M., "Leading-Edge Vortex Structure of Nonslender Delta Wings at Low Reynolds Number," *AIAA Journal*, Vol. 41, No. 1, 2003, pp. 16–26.

[3]Honkan, A., and Andreopoulos, J., "Instantaneous Three-Dimensional Vorticity Measurements in Vortical Flow over a Delta Wing," *AIAA Journal*, Vol. 35, No. 10, 1997, pp. 1612–1620.

[4]Miau, J. J., Kuo, K. T., Liu, W. H., Hsieh, S. J., Chou, J. H., and Lin, C. L., "Flow Developments Above 50-Deg Sweep Delta Wings with Different Leading-Edge Profiles," *Journal of Aircraft*, Vol. 32, No. 4, 1995, pp. 787–794.

[5]Gordnier, R. E., and Visbal, M. R., "Higher-Order Compact Difference Scheme Applied to the Simulation of a Low Sweep Delta Wing Flow," AIAA Paper 2003-0620, Jan. 2003.

[6]Taylor, G. S., Schnorbus, T., and Gursul, I., "An Investigation of Vortex Flows over Low Sweep Delta Wings," AIAA Paper 2003-4021, June 2003.

[7]Taylor, G. S., and Gursul, I., "Unsteady Vortex Flows and Buffeting of a Low Sweep Delta Wing," AIAA Paper 2004-1066, Jan. 2004.

[8]Yaniktepe, B., and Rockwell, D., "Flow Structure on a Delta Wing of Low Sweep Angle," *AIAA Journal*, Vol. 42, No. 3, 2004, pp. 513–523.

[9]Yavuz, M. M., Elkhoury, M., and Rockwell, D., "Near-Surface Topology and Flow Structure on a Delta Wing," *AIAA Journal*, Vol. 42, No. 2, 2004, pp. 332–340.

[10]Elkhoury, M., and Rockwell, D., 2003 "Visualized Vortices on Unmanned Combat Air Vehicle Planform: Effect of Reynolds Number," *Journal of Aircraft*, Vol. 41, No. 5, 2004, pp. 1244–1247.

[11]Elkhoury, M., Yavuz, M. M., and Rockwell, D., "Near-Surface Topology of Unmanned Combat Air Vehicle Planform: Reynolds Number Dependence," *Journal of Aircraft*, Vol. 42, No. 5, 2005, pp. 1318–1330.

[12]Wood, N. J., Roberts, L., and Celik, Z., "Control of Asymmetric Vortical Flow over Delta Wings at High Angles of Attack," *Journal of Aircraft*, Vol. 27, No. 5, 1990, pp. 429–435.

[13]McCormick, S., and Gursul, I., "Effect of Shear Layer Control on Leading Edge Vortices," *Journal of Aircraft*, Vol. 33, No. 6, 1996, pp. 1087–1093.

[14]Gu, W., Robinson, O., and Rockwell, D., "Control of Vortices on a Delta Wing by Leading-Edge Injection," *AIAA Journal*, Vol. 31, No. 7, 1993, pp. 1177–1186.

[15]Vorobieff, P., and Rockwell, D., "Vortex Breakdown on Pitching Delta Wing: Control by Intermittent Trailing Edge Blowing," *AIAA Journal*, Vol. 36, No. 4, 1998, pp. 585–589.

[16]Parmenter, K., and Rockwell, D., "Transient Response of Leading Edge Vortices to Localized Suction," *AIAA Journal*, Vol. 28, No. 6, 1990, pp. 1131–1133.

[17]Johari, H., Olinger, D. J., and Fitzpatrick, K. C., "Delta Wing Vortex Control via Recessed Angled Spanwise Blowing," *Journal of Aircraft*, Vol. 32, No. 4, 1995, pp. 804–810.

[18]Helin, H. E., and Warty, C. W., "Effects of Trailing Edge Entrainment on Delta Wing Vortices," *AIAA Journal*, Vol. 32, No. 4, 1994, pp. 802–804.

[19]Shih, C., and Ding, Z., "Trailing Edge Jet Control of Leading Edge Vortices of a Delta Wing," *AIAA Journal*, Vol. 34, No. 7, 1996, pp. 1447–1457.

[20]Mitchell, A. M., Molton, P., Barberis, D., and Delery, J., "Control of Leading Edge Vortex Breakdown by Trailing Edge Injection," AIAA Paper 99-3202, 1999.

[21]Phillips, S., Lambert, C., and Gursul, I., "Effect of a Trailing-Edge Jet on Fin Buffeting," *Journal of Aircraft*, Vol. 40, No. 3, 2003, pp. 590–599.

[22]Wang, J. J., Li, Q. S., and Liu, J. Y., "Effects of Vectored Trailing Edge Jet on Delta Wing Vortex Breakdown," *Experiments in Fluids*, Vol. 34, May 2003, pp. 651–654.

[23]Legendre, R., "Lignes de Courent d'un Ecoulement Continu," *La Recherche Aérospatiale*, No. 105, 1965, pp. 3–9.

[24]Perry, A. E., and Hornung, H. G., "Some Aspects of Three-Dimensional Separation. Part II. Vortex Skeletons," *Z.Flugwiss.Weltraumforsch*. Vol. 8, 1984, pp. 155–160.

[25]Perry, A. E., and Chong, M. S., "A Description of Eddying Motions and Flow Patterns Using Critical-Point Concepts," *Annual Review of Fluid Mechanics*, Vol. 19, 1987, pp. 125–155.

[26]Dallman, U., and Schulte-Werning, B., "Topological Changes of Axisymmetric and Non-Axisymmetric Vortex Flows," *Topological Fluid Mechanics, Proceedings of the IUTAM Symposium*, edited by H. K. Moffat and A. Tsinober, Cambridge Univ. Press, Cambridge, England, U.K., 1990, pp. 372–383.

[27]Su, W., Liu, M., and Liu, Z., "Topological Structures of Separated Flows About a Series of Sharp-Edged Delta Wings at Angles-of-Attack up to 90°," *Topological Fluid Mechanics*, *Proceedings of the IUTAM Symposium*, edited by H. K. Moffat and A. Tsinober, Cambridge Univ. Press, Cambridge, England, U.K., 1990, pp. 395–407.

[28]Lazos, B., "Surface Topology on the Wheels of a Generic Four-Wheel Landing Gear," *AIAA Journal*, Vol. 40, No. 12, 2002, pp. 2402–2412.

K. Ghia
Associate Editor